Enhancement of Parameters of Slotted Waveguide Antennas Using Metamaterials

Minu Valayil [1] and Kent Chamberlin [2]

[1] SI2 Technologies; mvalayil@si2technologies.com
[2] University of New Hampshire, Dept. of ECE; kent.chamberlin@unh.edu

Abstract **-** An approach to increasing the gain of a slot-array antenna through the use of metamaterials is presented. The specific array antenna used in this study is a 2x4 resonant, slotted-waveguide array, although the results presented should be applicable to most arrays with slot radiators. To achieve increased gain, a metamaterial structure comprised of a split-ring resonator in conjunction with a wire structure was placed above the radiating slots. Modeled results for this configuration predicted an increase in directivity of 49%, and this result was subsequently validated by fabricating and performing measurements on antenna arrays incorporating the metamaterials. The increase in directivity also resulted in increased efficiency and sidelobe depth and yet did not degrade return loss. The measured results show that the maximum gain enhancement of antennas with metamaterials increased by up to 58% with respect to the control antenna which did not employ metamaterials.

Index Terms **-** antenna measurement, antenna modeling, beamwidth, metamaterials, slotted antenna, split-ring resonator.

I. INTRODUCTION

In the work reported here, metamaterial structures were placed above the radiating slots in a slotted waveguide antenna (SWA) array to increase the gain of the array without increasing its physical size. The results, both measured and modeled, show that a modest increase in gain is achievable by using metamaterials.

In an approach similar to the one presented here, Nicholson et al. [1] explored the use of split-ring resonators (SRR), which behave as metamaterial structures, to couple energy through a resonant slot in the waveguide. Their work was based on simulations, and they reported that the approach showed potential improvement in gain. However, their focus was to achieve improvement of structural properties by reducing the slot length through the use of a single SRR for each slot [1]. Although the approach presented here is similar to the approach of Nicholson, et al., there are two significant differences. One is that the metamaterial used here includes a wire structure in addition to the SRR. The other difference lies in the placement of the metamaterial structure. Specifically, their SRR was positioned in the radiating slot, while the metamaterial used here was positioned above the slot. The likely advantages to this revised metamaterial placement are that it will be less complicated to assemble, and it will provide greater bandwidth. Another recent paper introduced three split resonators inside the waveguide to yield high gain and front-to-back radiation ratio [17]. Again, this is also another application of the SRRs inside a waveguide but not on the outside of slotted waveguide antenna. Our application of SRRs on the outside of the slotted waveguide enhanced the directivity and gain compared to that of a conventional slotted waveguide antenna.

Computer modeling results using the metamaterial structure and placement described above predicted an increase in directivity [2]. To validate those modeled results, and to explicitly evaluate the effects of metamaterials on array performance, three 2x4 slot arrays were modeled, fabricated and measured. One was a conventional resonant-slot antenna, used as a control. The other two antennas were slot arrays of nearly identical design, having metamaterial structures positioned above their slots in an orientation that maximized the coupling between the metamaterial and the slot. That maximum coupling occurs when the metamaterial structure is either parallel to the slot or at right angles to it. As is detailed below, there were small variations in the slot dimensions and location for the three antenna arrays, and those variations were necessary to make the antennas identical electrically in terms of slot impedance.

The agreement between measured and modeled data was reasonable for the three configurations, and those results show an increase in directivity and concomitant decrease in beamwidth for both of the metamaterial orientations. The modeling software, High Frequency Structure Simulator (HFSS) by Ansys, showed a gain equal to directivity since the waveguide was modeled using Perfect Electric Conductor (PEC) boundaries. Because of this, the modeled directivity, rather than the modeled gain, is used in this study. The antennas were optimized using the model to achieve best directivity, return loss and lower sidelobes.

II. MATERIALS AND METHODS

2.1 Resonant Slot Array Antenna

All three arrays studied used a half-height WR-90

Submitted On: August 15, 2018
Accepted On: December 24, 2018

(0.9in x 0.2 in) rectangular waveguide as their input, with wall thickness of 0.050in. They were designed to be operational over the frequency band of 9.3 to 9.7GHz. The 8 slots were $\lambda_g/2$ apart with shorted ends and thus perform as linear, resonant, slotted-waveguide antenna arrays. The control antenna, the one without the metamaterials, is shown in Fig. 1 and was designed using Elliott's technique [3], although a computer model was used to fine tune slot impedances.

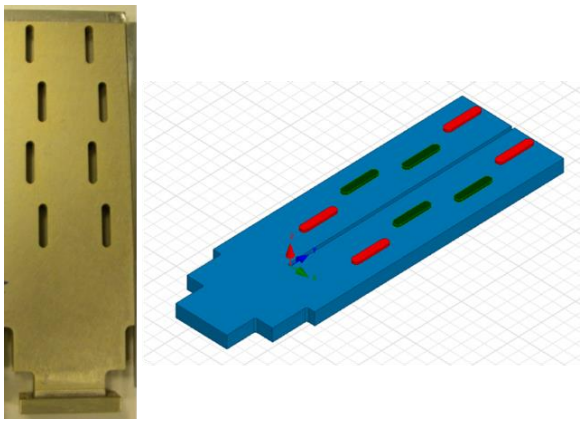

Fig. 1. The control antenna is a conventional 2x4 slot-array design without metamaterial structures: the array is pictured on the left and the array as modeled in HFSS is shown on the right.

The waveguide used to feed the arrays has an "a" dimension of 0.864in and a "b" dimension of 0.2in. As seen in Fig. 1, the slots are placed on the broadside of the waveguide and are separated by a distance compatible with TE_{10} mode operation. The offsets and slot dimensions were optimized using HFSS to minimize return loss. Minimal return loss will occur when the admittance of each slot is purely real and the total admittance is equal to characteristic impedance of the waveguide [4]. The slot dimensions for the finalized design of the control antenna are given in Table 1.

Table 1: Dimensions for the control slotted-waveguide array

Dimension	Offset (in)	Length (in)
Slot 1	0.08	0.610
Slot 2	0.09	0.615
Slot 3	0.09	0.615
Slot 4	0.08	0.610
Short distance	0.374	
Slot width	0.126	
Guide wavelength (λ_g)	0.894	

2.2 *Metamaterial Resonant Slot Array Design*

Metamaterial Design: In 1964 Veselago introduced the possibility of negative-refractive-index materials that had no known existence in nature [5] at that time. He proposed the possibility of configuring materials so as to create a structure with a negative refractive index [5]. Several practical designs employing metamaterial structures exist today: Zhang and Deng [6] introduced a metamaterial transmission line structure with split-ring resonators (SRRs) along with complimentary split-ring resonators (CSRRs). Smith et al. demonstrated that a SRR in conjunction with a wire structure would introduce negative permeability and negative permittivity [7].

The metamaterial structure used in this work, referred to as a unit cell and depicted in Fig. 2, follows the work by Smith by including both a SRR and a wire structure to create the metamaterial. The dimensions for the components comprising the unit cell were adjusted to achieve resonance at 9.5GHz as described below.

Unit cells can be joined with other unit cells to increase the physical size of the metamaterial and for the work presented, three co-linear unit cells where shown to provide the best results.

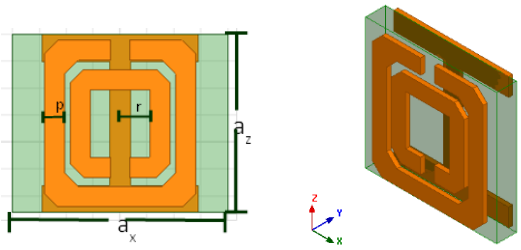

Fig. 2. A single unit cell of metamaterial structure used for this application, consisting of a SRR on the top layer of the substrate and the wire structure on the bottom layer.

The overall size of the unit cell SRR and the wire structure is 3.31mm x 3.31mm x 0.5mm and was fabricated on RO5880 substrate. The dimensions were determined using the Lorentz model for a SRR and the Drude model for the wire structure [8]. Dimensions for the unit cell structures can also be calculated using equations published by Engheta et al. [9].

Using the dimensions from the models given above, the unit cell was modeled in HFSS to assess its performance characteristics as described below. Achieving resonance at the desired frequencies required iterating the design with HFSS, and the dimensions identified in that process are given in Table 2.

Table 2: The unit cell dimensions to achieve resonance at 9.5GHz; rough values were calculated using the Drude and Lorentz models, and those values were refined using a computer model to yield the results given above

Variables	Dimensions (mm)
p	0.375
r	0.83
a_x	3.31
a_y	3.31

The configuration used to model the unit cell in HFSS is shown in Fig. 3, where the input and output ports are created using the software's waveport function; those ports are shown on the left and right faces of the computational space given in Fig. 3. In this particular configuration, the Poynting vector will flow parallel to both the SRR and wire structure, with the fields oriented as shown in Fig. 3. The effect of the unit cell on the excitation is given by the waveport's S parameters, which are plotted in Fig. 4.

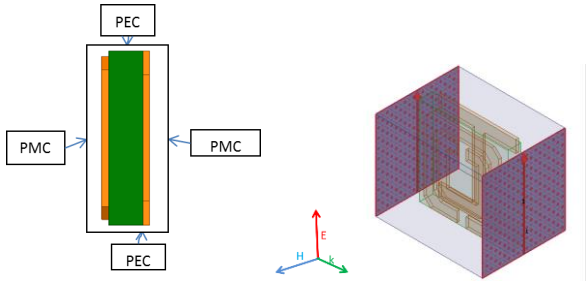

Fig. 3. Unit cell configuration modeled in HFSS: side view (left) and a projection of the 2-port waveport excitation set-up.

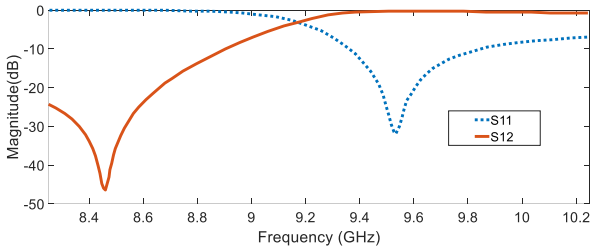

Fig. 4. HFSS S-parameter plot of the unit cell.

The modeled unit-cell S-parameters are plotted in Fig. 4, showing a magnetic-field resonant frequency of approximately 8.5GHz and a resonance frequency at 9.5GHz [8, 10]. Referring to Fig. 4, the closest impedance match appears to be in the range of 9.4 to 9.7GHz, which is coincident with the slotted waveguide antenna resonant frequency. The following section uses the data in Fig. 4 to extract the effective permittivity and permeability, showing that they are both negative within the frequency range of interest.

The orientation of the unit cell with respect to the excitation source as shown in Fig. 3 is analogous to positioning the unit cell at right angles to the plane of the slot. This orientation for the unit cell is one of the orientations investigated in this study. The other is where the unit cell is rotated 90° such that the plane of the cell is parallel with the right face. This rotated configuration was modeled as well and provided nearly identical results to the orientation of Fig. 3, and the enhancement to antenna performance was also nearly the same for both orientations.

Metamaterial Characterization: The objective of this section is to show that the unit cell used in this study behaves as a metamaterial. This is accomplished using the S-parameters plotted in Fig. 4 to determine the cell's effective permittivity and permeability.

A number of approaches exist in the literature to extract electromagnetic properties of a medium: (1) field averaging (2) curve-fitting (3) the dispersion equation and (4) S parameters [11]. The S-parameter method is commonly used for this purpose.

Several methods of S-parameter extraction techniques have been developed to characterize metamaterial structures. Those include (1) Nicholson-Ross-Weir (NRW) method (2) Bloch-Floquet Theorem method. Ziolkowski uses NRW method in his paper to retrieve effective medium parameters [8]. However, the paper by Nicholson et al. shows some limitations regarding the usage of the method for narrow bandwidth [6]. Consequently, the Bloch-Floquet method is used here to retrieve the essential parameters. The fundamental mode, TE_{10}, is the only mode considered here.

Palandoken et al. describes the Bloch-Floquet method used for extracting the parameters plotted below [13]; calculated effective permeability (μ_{eff}) and effective permittivity (ϵ_{eff}) are given in Figs. 5 and 6, respectively. As seen in Fig. 5, the real part of the permeability is negative in the frequency range between the magnetic resonance at 9.18GHz and the plasma frequency at about 11GHz. The permeability curve shows that the highest magnetic loss is close to the magnetic resonance frequency of 8.5GHz.

The magnetic resonance seen at 8.46GHz in Fig. 4 is coincident with the resonance in the permeability and permittivity curves shown in Figs. 5 and 6, respectively. The imaginary part of the effective permittivity shown in Fig. 6 is negative in the frequency range of about 8.25GHz to9.1 GHz. The Drude type response is seen to be in the frequency range of around 8.5 to 9.2GHz as is

expected for a wire structure [14]. This response agrees well with the results published by Liu et al. [15].

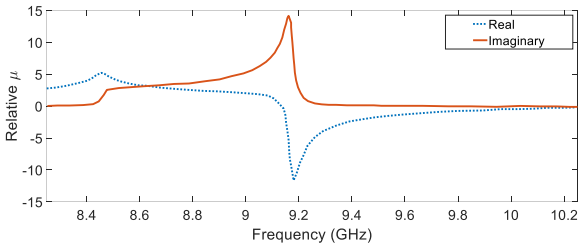

Fig. 5. The real and imaginary part of the effective permeability of the unit cell.

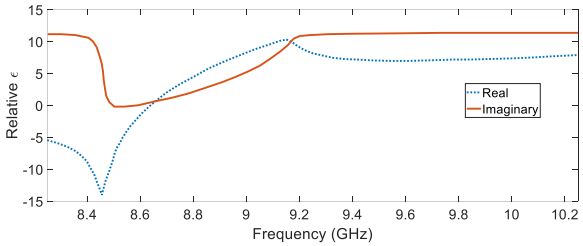

Fig. 6. The real and imaginary part of the effective permittivity of the unit cell.

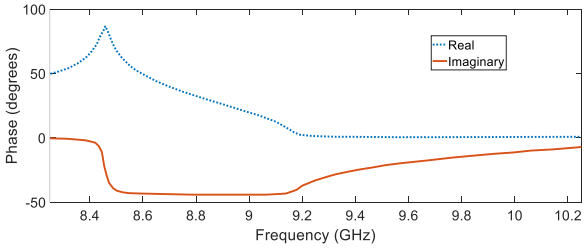

Fig. 7. The real and imaginary part of the phase of the unit cell.

Based upon the effective permittivity and permeability plots above, the unit cell in this paper can be represented as a Lorentz-Drude model [15]. The phase diagram, given in Fig. 7, shows the bandgap region in the same frequency range where the real part of permittivity is negative and the real part of the permeability is positive [10]. This bandgap region is also evident in the S-parameter result in Fig. 4.

As seen in Figs. 6 and 7, the combination of the SRR and wire structure has a clearly defined frequency range where both the permittivity and permeability are negative. Smith, et al. [16] has shown that this characteristic defines metamaterials, and hence it can be concluded that the structure used in this study behaves as a metamaterial.

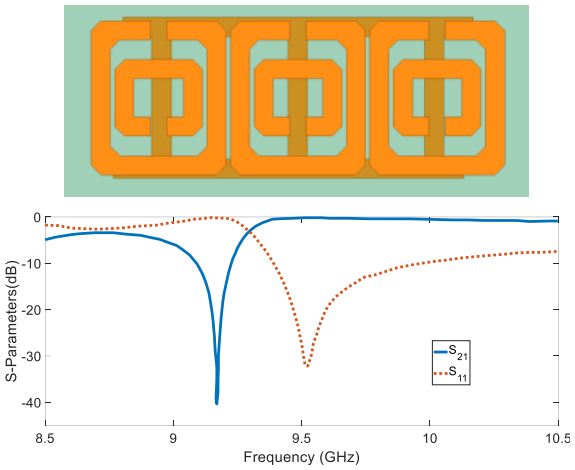

Fig. 8. Top: array of three elements used for the application. Bottom: the HFSS S-parameter results of metamaterial array.

As stated above, multiple unit cells can be added together to create a metamaterial of larger area. For this study, three elements, as shown in Fig. 8, proved to be of sufficient size to interact with the array slots. Modeled results using four elements together showed distortion in the radiation pattern and hence the use of a larger number of unit cells was not explored further.

The gap between the individual unit cell structures is crucial, and modeling results showed the optimal gap size to be 0.004". This gap size was used in the fabrication of the cells. The dimension of the SRR and the wire is the same as that of the unit cells. The wire structure on either side of the middle SRR is offset by about 0.001" since this proved to yield the greatest directivity in simulations. The array was fabricated on a 3.1 mil Rogers 5880 substrate with ϵ_r of 2.2 and dielectric loss tangent of 0.0009. The thickness of the copper deposition is 1 oz. on both sides of the substrate. When compared to the S-parameter results of a single unit cell in Fig. 4, the results for the three-unit-cell configuration show the S_{21} resonance at 8.46GHz is shifted to 9.17GHz, closer to the desired resonance frequency at 9.5GHz. These two resonances, the electric and the magnetic, reappear in the S-parameter results of the array as shown in Fig. 10. Those resonances occur at approximately 8.75GHz and 9.6GHz, respectively.

The array three-unit-cell metamaterial structure was evaluated by orienting it two different ways, one vertical with respect to the slots and the other horizontal to the slots. Either orientation appears to give approximately the same benefits in terms of increasing gain, directivity and narrowing the beamwidth.

2.3 Orienting the Metamaterial Structures Vertically with Respect to the Slots

In the vertically-oriented configuration, the three-unit-cell metamaterial structure was positioned over each of the radiating slots as shown in Figs. 9 (a) and 9 (b), where the plane of the cell is at right angles to the plane of the slot. The middle SRR of the array of metamaterial structures is located at the center of the slots. The height of the metamaterial structures was optimized to give the maximum gain.

Introduction of the metamaterial structure over the slots changed the impedance of the slots. To compensate for those changes, the computer model was used to estimate slot dimensions that would be matched for this particular slot-metamaterial configuration. By optimizing slot match, the return loss was also minimized. Those new dimensions are given in Table 3 and were used in fabricating the antenna array for the vertically-oriented metamaterial tests.

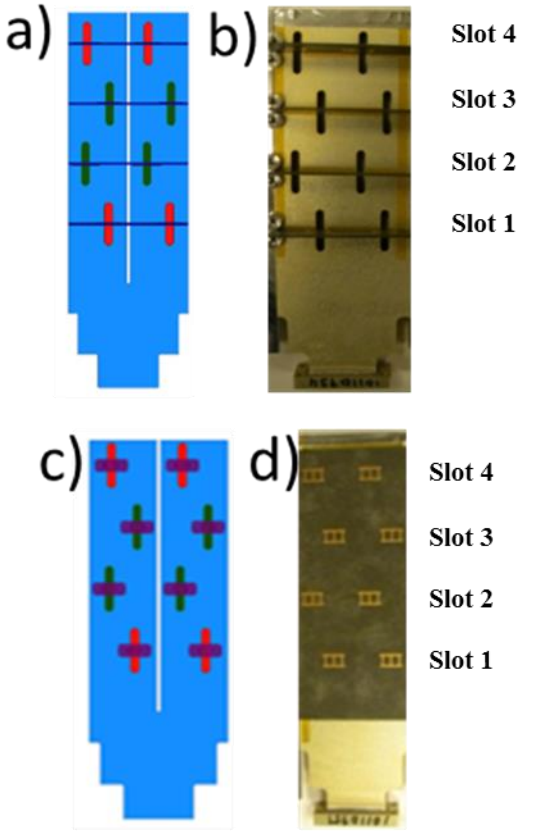

Fig. 9. (a) HFSS model representation of slotted waveguide with metamaterial structures mounted vertically, (b) picture of fabricated prototype of the vertically mounted metamaterial structure, (c) HFSS model of the horizontally-mounted metamaterial on top of the array slots, and (d) picture of fabricated prototype of horizontally mounted metamaterial structures

Table 3: Array dimensions to achieve matched slots for the vertically-mounted and horizontally-mounted metamaterial structure

	Vertically Mounted		Horizontally Mounted	
Dimension	Offset (in)	Length (in)	Offset (in)	Length (in)
Slot 1	0.16	0.64	0.16	0.665
Slot 2	0.18	0.65	0.18	0.675
Slot 3	0.18	0.65	0.18	0.675
Slot 4	0.16	0.64	0.16	0.66
Short distance	0.44		0.36	
Slot width	0.12		0.11	
Distance of SRR structures from slot	0.135		0.15	
Guide wavelength (λ_g)	0.894		0.894	

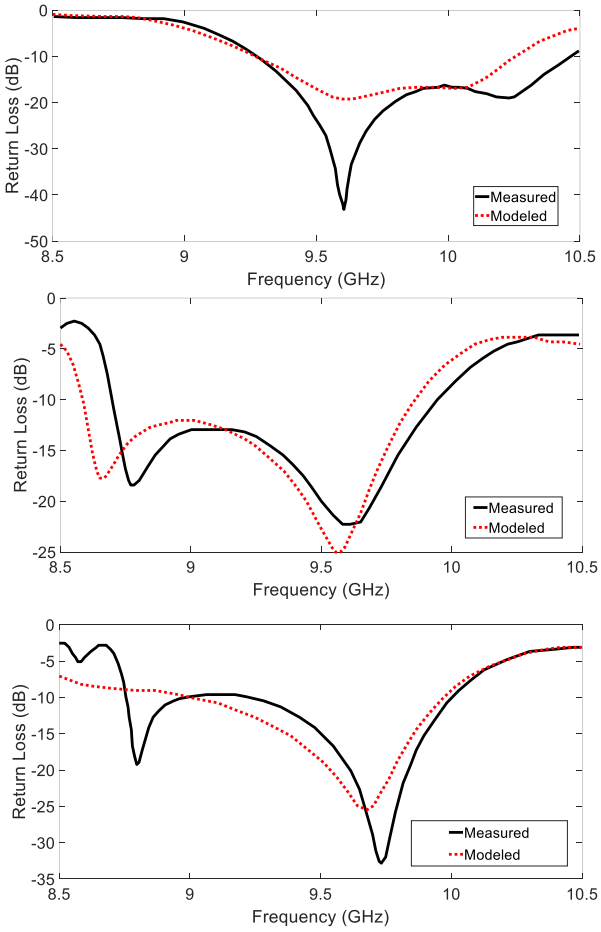

Fig. 10. Measured and modeled return loss for: control antenna (top), metamaterial mounted vertically (middle) and metamaterial mounted horizontally (bottom).

2.4 Orienting the Metamaterial Structures Horizontally with Respect to the Slots

In the horizontally-oriented configuration, the same three-unit-cell metamaterial structure was used, although its physical orientation was rotated by 90° as shown in Figs. 9 (c) and 9 (d). This configuration was optimized to minimize return loss, resulting in the array dimensions

given in Table 3. As with the vertically-oriented metamaterial configuration, the middle SRR of the array of metamaterial structures was located at the center of the slots. The height of the metamaterial structures was optimized to give the maximum gain.

III. RESULTS

The three antenna arrays described above were manufactured at Cobham Advanced Electronic Solutions, Exeter, NH to validate the modeled results. Those arrays were fabricated using the design parameters described above.

The far-field measurements were collected in a near-field anechoic chamber with NSI test set-up using a cylindrical scanner in a manner consistent with industry standards.

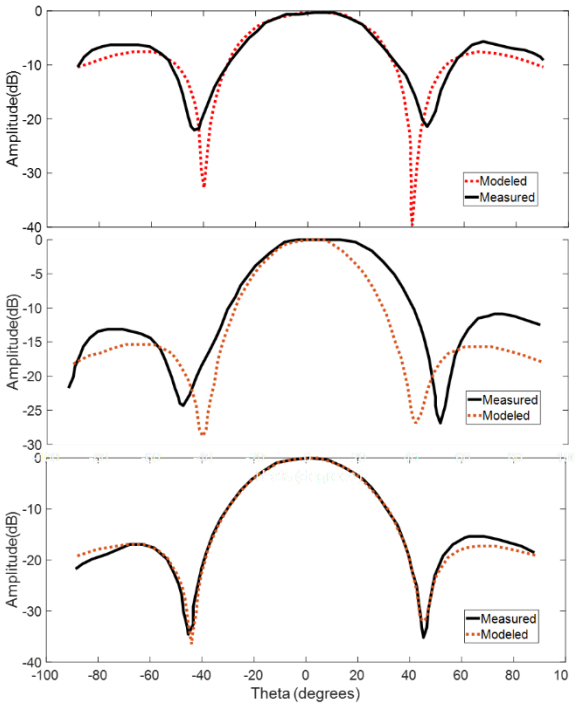

Fig. 11. E-Field radiation patten for the three antenna array configurations: control (top), vertical (middle) and horizontal at 9.6GHz.

3.1 Measured and Modeled Return Loss

The return-loss graphs for the three antenna arrays, given in Fig. 10 show reasonable agreement between the simulated and measured data for the frequencies of interest (9.3 to 9.7GHz). A conclusion that can be drawn from the S-parameter data in those figures is that all three arrays are viable from an impedance match perspective.

The return loss measurements for all three antennas showed the best match at 9.6GHz, and thus the radiation patterns were measured at that frequency.

3.2 Measured and Modeled Radiation Patterns

The modeled and measured radiation pattern data for the E-plane and H-plane at 9.6GHz for the three antennas are plotted in Figs. 11 and 12. As seen in the figure, there is reasonable agreement between the model and measurements for the three configurations. The sidelobes of the metamaterial antennas are suppressed more than the control antenna by 10dB.

There is an anomaly in the results that should be noted here. The vertically-oriented metamaterial antenna has a somewhat distorted pattern when compared to the simulated in E-plane as can be seen in Fig. 11. The assumed reason for this difference is that the metamaterial structure is flexible and was observed to be slightly curved during the test. A close examination of Fig. 3 (a) appears to confirm this assumption. Consequently, it is reasonable to assume that both metamaterial structure orientations will provide identical results if the metamaterial structures are mounted correctly.

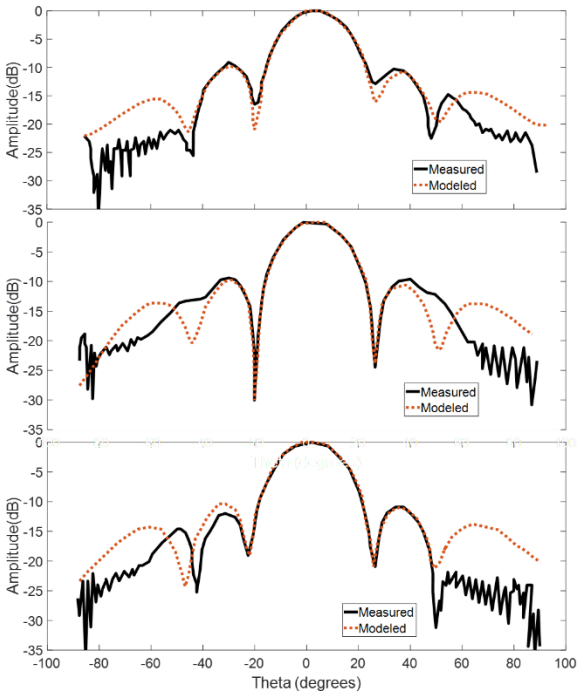

Fig. 12. H-Field radiation patten for the three antenna array configurations: control (top), vertical (middle) and horizontal at 9.6GHz.

3.3 Array Gain and Efficiency

The gain versus frequency plot of Fig. 13, which was generated using measured data, shows the variation in gain over the frequency range of 8.5 to 10.5GHz. The gain of the control array is seen to be greater than 14dB in the frequency range of 9.4 to 9.9GHz. This value increases to 14.9dB in the range of 9.9 to 10.5GHz, resulting in a bandwidth of 1100MHz. The array with the hor-

izontally-oriented metamaterial also shows a gain greater than 14dB in the frequency range of 8.9 to 10.3GHz, resulting in a bandwidth of 1400MHz, or about 300MHz more than the control antenna. The array with the vertically-oriented metamaterial shows nearly the same bandwidth as the array with the horizontally-oriented metamaterial.

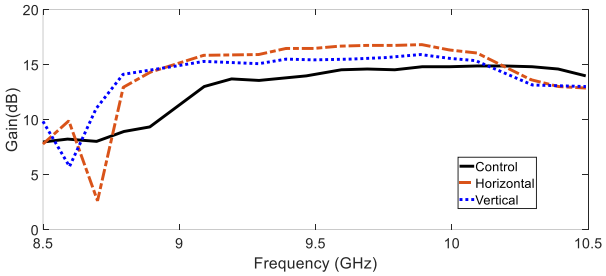

Fig. 13. Plot of gain versus frequency, calculated using measured data.

Referring to Fig. 13, the gain difference between the control array and the array with the horizontally-oriented metamaterial is approximately 2dB and this difference exists over a frequency span of nearly 1000MHz. Also evident in Fig. 13 is a gain difference of 0.9dB between the array with the vertically-oriented metamaterial and the array with the horizontally-oriented metamaterial due to some axial deformation in the metamaterial structure as described above. Based on the efficiency plot shown below in Fig. 14 proves that the efficiency of both the horizontal and the vertical mounted metamaterial antenna is better than the conventional slotted waveguide antenna.

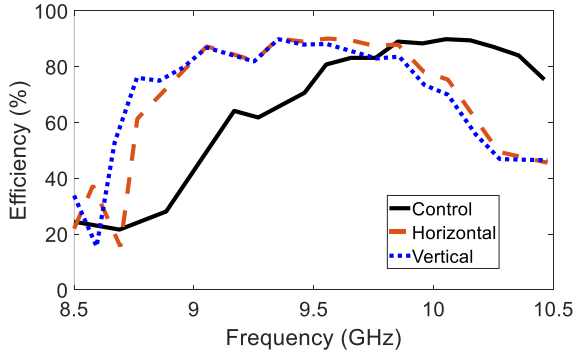

Fig. 14. Plot of efficiency versus frequency calculated using measured data.

IV. DISCUSSION AND CONCLUSIONS

The finding of the work described above is that a modest, approximately 2 dB over a wide bandwidth, increase in gain can be achieved by placing a metamaterial structure over the radiating slots in a slotted-array antenna. This can be achieved without increasing the physical size of the antenna, and the cost to include the metamaterial design presented here in the final product should be minimal.

There appears to be several mechanisms at play that cause the metamaterials to bring about the increased gain. One is that the metamaterial structure increases coupling through the slots by placing them in the reactive near-field of the slots.

Another explanation for the increased gain is that the negative index of refraction of the metamaterials compensates for the diffraction that occurs as the wave exits the waveguide slots. If diffraction compensation does occur, it would likely enhance coupling through the slot and bring about the lesser reflection mentioned in the previous paragraph. Diffraction compensation would also tend to provide a lens-like focusing of the energy which would increase directivity as reported in [7].

V. PATENTS

M. Valayil, inventor; Continental Microwave & Tool Co., Inc dba Cobham Advanced Electronic Solutions, assignee. Slotted waveguide antenna with metamaterial structures. US patent 9,595,765B1. 2017 March 14.

ACKNOWLEDGMENT

This work is funded by Cobham Advanced Electronic Solutions, Exeter, NH. Special thanks to Peter Beaulieu, Dr. Yun-Li Hou, James Skladany, Dr. Mahesh Kumar and Dan Wall at Cobham for insightful discussion on this topic.

REFERENCES

[1] K. Nicholson, W. Rowe, and P. Callus, "Split-ring resonator loaded slot array," Proceedings of the Asia-Pacific Microwave Conference, pp. 1338-1341, 2011.

[2] M. Valayil and K. Chamberlin, "Enhancement of antenna parameters of slotted waveguide antenna using metamaterials," IEEE APS-URSI, 2014.

[3] W. Zhang, Y. Zhao, and M. Zhang, "The synthesis of a longitudinal slot array on a rectangular waveguide," IEEE, vol. 12, pp. 202-205, 2012.

[4] M. Orefice and R. S. Elliott, "Design of waveguide-fed series slot arrays," IEEE PROC., vol. 129, August 1982.

[5] V. G. Veselago, "The electrodynamics of substances with simultaneously negative values of ϵ and μ," Sov. Phys., vol. 10, pp. 509-514, January 1968.

[6] Y. Zhang and L.-L. Deng, "Metamaterial transmission lines based on split-ring resonators (SRRs) and complementary split ring resonators (CSRRs)," ICMMT 2010 Proceedings, pp. 2075-2077, 2010.

[7] D. R. Smith, D. Shurig, and J. B. Pendry, "Negative refraction of modulated electromagnetic waves," Applied Physics Letters, vol 81, 2713, 2002.

[8] R. W. Ziolkowski, "Design, fabrication, and testing of double negative metamaterial," Antennas and Prop. IEEE, vol. 51, 2003.

[9] N. Engheta and R. W.Ziolkowski, "A positive future for double-negative metamaterials," IEEE Trans. Microwave Theory and Tech., vol. 53, 2005.

[10] V. Varadan and A.Tellakula, "Effective properties of split-ring

resonator metamaterials using measured scattering parameters: Effect of gap orientation," Journal of Applied Physics, vol. 100, 2006.

[11] S. Arslanagic, T. V Hansen, N. A Mortensen, A. H Gregersen, O. Sigmund, R. W. Ziolkowski, and O. Breinbjerg, "A review of the scattering parameter extraction method with clarification of ambiguity issues in relation to metamaterial homogenization," IEEE A&P Magazine 55(2), 91-106, 2013.

[12] A. M. Nicolson and G. F. Ross, "Measurement of the intrinsic properties of materials by time domain techniques," IEEE Trans. Instrum. Meas., vol. IM-19, pp. 377-382, Nov. 1970.

[13] M. Palandoken and H. Henke, "Fractal spiral resonator as magnetic metamaterial," IEEE, 09, 2009.

[14] D. R. Smith, "Analytic expressions for the constitutive parameters of magnetoelectric metamaterials," Physical Review, vol. 81, 2010.

[15] R. Liu, T. J. Cui, B. Zhao, D. Huang, and D. R. Smith, "Description and explanatin of electromagnetic behaviors in artificial metamaterials based on effective medium theory," Phys. Rev., vol. 76, 2007.

[16] D. R. Smith, S. Schultz, P. Markos, and C. M. Soukoulis, "Determination of negative permittivity and permeability of metamaterials from reflection and transmission coefficients," Phys. Rev. B, 65, 2002.

[17] A. Chandra and S. Das, "Application of SRR to achieve performance improvement and multiband characteristics in aperture antennas," IET Microwaves, Antennas & Propogation, vol. 11, pp. 990-996, 2017.

Minu Valayil is a Principal Engineer at SI2 Technologies, where she is focused on antenna design and development of new antenna technologies. She has 9 years of experience in the field of Electrical Engineering as an Microwave/RF Engineer, with 2 years of Antenna Engineering experience. Valayil's work at SI2 has been focused on the design and development of broadband, electrically small, and structurally integrated antennas and arrays. Prior to joining SI2, Valayil worked as a RF/Microwave Engineer at Cobham Integrated Electronic Solutions (CIES), in Exeter, NH. She received Sir Alan Cobham Bronze Award for Innovation for her development of metamaterial application on slotted waveguide antenna systems.

Valayil received her M.S. in Electrical Engineering from University of New Hampshire with a concentration on metamaterial antennas and BS degrees in Electrical Engineering and Biomedical Engineering from Letourneau University, Longview, TX.

Kent Chamberlin is the Chair and a Professor in the Department of Electrical and Computer Engineering. In his more than thirty-five years in academia, he has performed research for more than twenty sponsors, including the National Science Foundation. He has received two Fulbright awards, including the Fulbright Distinguished Chair, which he served in Aveiro, Portugal. He has also served as an Associate Editor for the Institute for Electrical and Electronics Engineers, and he continues to be active in performing and publishing in a range of research areas.